

The tectonic development of the Central African Plateau: evidence from shear-wave splitting

R. Kounoudis,¹ J.-M. Kendall,¹ C.S. Ogden,² S. Fishwick,² C. Chifwepa³ and M.C. Daly¹

¹Department of Earth Sciences, University of Oxford, Oxford, OX1 3AN, UK. E-mail: rita.kounoudis@earth.ox.ac.uk

²School of Geography, Geology and the Environment, University of Leicester, Leicester, LE1 7RH, UK

³Geological Survey Department, Ministry of Mines, Lusaka, P.O Box 31969, Zambia

Accepted 2024 September 18. Received 2024 September 18; in original form 2024 August 5

SUMMARY

The Central African Plateau comprises a mosaic of numerous Archean terranes—the Congo, Bangweulu and Kalahari Cratons—sutured in a series of Proterozoic to early Cambrian orogenic events. Major upper-crustal deformation and complex craton margin fault zones reflect the region's diverse tectonic history: rifting during the Neoproterozoic, collision during the Pan-African orogeny, and more recently, Permo-Triassic Karoo rifting and the Pliocene development of the Southwestern branch of the East African Rift. The tectonic evolution and extent to which the lithospheric mantle has been re-worked by each tectonic event is poorly understood. New seismograph networks across the Plateau provide fresh opportunity to place constraints on the plate-scale Precambrian-to-Phanerozoic processes that have acted across the region. Utilizing data from seismograph deployments across the Central African Plateau, including the new Copper Basin Exploration Science network—a NW–SE-trending, 750-km-long profile of 35 broad-band stations—we explore lithospheric deformation fabrics associated with past and present tectonic events via a shear-wave splitting study of mantle seismic anisotropy. Results reveal short length-scale variations in splitting parameters (fast direction: ϕ , delay time: δt), suggestive of a fossil lithospheric fabric cause for the observed anisotropy. A lack of fault-parallel ϕ across the Mwembeshi shear zone, suggests it may be too narrow at mantle depths, a thin-skinned, crustal-scale feature, and/or did not experience sufficient fault parallel shear-strain during its last active phase to form a lithospheric deformation fabric discernible via teleseismic shear-wave splitting. In the heart of the Lufilian Arc, we observe abrupt changes in splitting parameters with NE–SW, N–S and NW–SE ϕ and $0.5 \text{ s} < \delta t < 1.2 \text{ s}$ evident at short length-scales: no single, uniform, anisotropic lattice preferred orientation (LPO) fabric defines the entire region. This is consistent with the view that multiple episodes of deformation shaped the Lufilian Arc, or perhaps that pre-existing fabrics, relating to Neoproterozoic Katangan Basin development, have failed to be completely overprinted by the Pan-African orogeny. Near the Domes, where most intense crustal re-working is thought to have taken place during the Pan-African orogeny, there is a cluster of null and low δt splits which likely reflects the lack of organized LPO fabrics, perhaps due to the presence of depth-dependent anisotropy. The neighbouring Congo Craton margin is marked by consistently weak anisotropy ($\delta t < 0.7 \text{ s}$) indicating a weak horizontal alignment of olivine at mantle lithospheric depths, typical of several Archean terranes worldwide.

Key words: Africa; Body Waves; Seismic Anisotropy; Mantle Processes; Cratons; Dynamics of Lithosphere and Mantle.

1 OVERVIEW

The Central African Plateau (Fig. 1a) documents tectonic events spanning 2 billion years of Earth history. Archean cores are stitched together through a series of Precambrian orogens—most notably, the

Pan-African orogeny—that culminated in the assembly of Gondwana (e.g., Porada & Berhorst 2000; Eglinger *et al.* 2016; Daly *et al.* 2020). The two main Pan-African orogenic belts across the Plateau are the Lufilian and Zambezi belts (Fig. 1a), both overprinting previous Neoproterozoic rift basins. The arcuate shape of

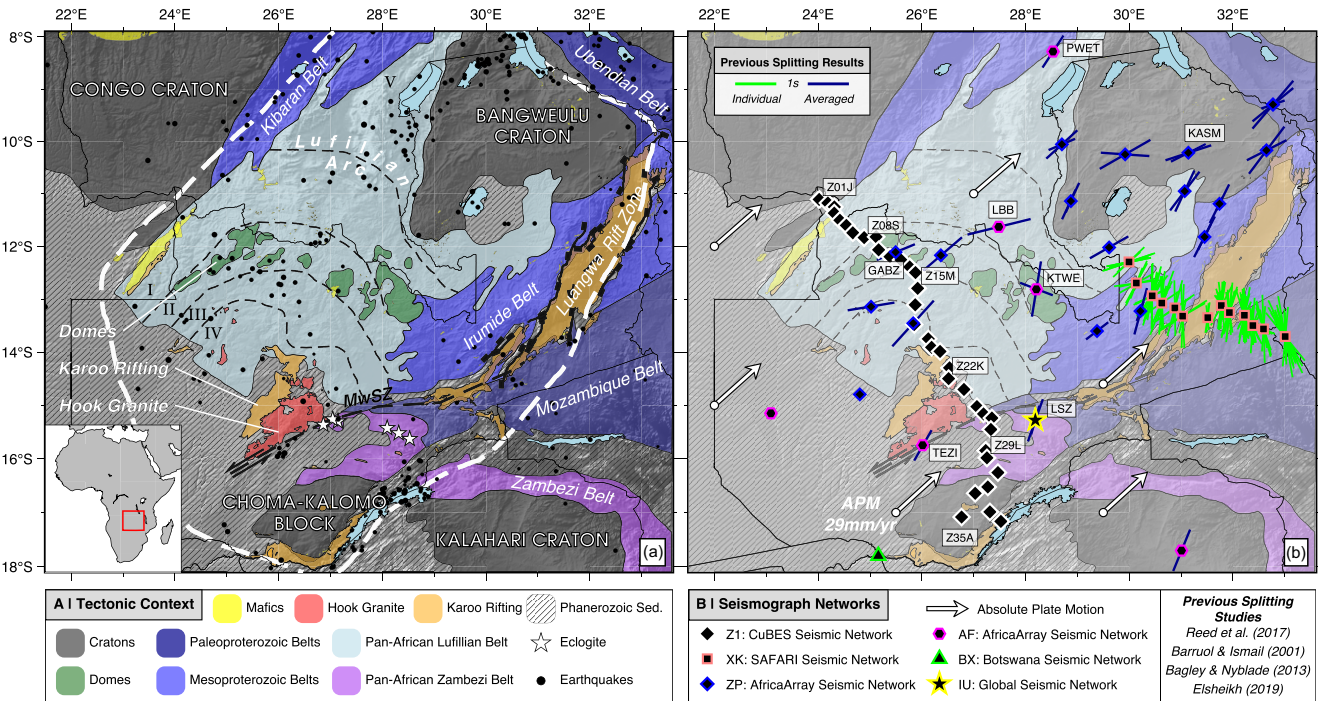


Figure 1. (a) Geology and tectonics of the Central African Plateau and surrounding regions. Tectonic units were taken from Thieme & Johnson (1981) and Xu *et al.* (2022). Active faults of the Luangwa Rift Valley are from Wedmore *et al.* (2022). Circles are earthquakes from 1964–present, recorded on the USGS catalogue. Zones labelled I–V show the main five tectonic subdivisions of the Lufilian Arc described by Porada (1989). The thick dashed line denotes the outline of the Central African Plateau as defined by Daly *et al.* (2020). MwSZ: Mwembeshi shear zone. (b) The 2022–2023 CuBES broad-band seismograph network and other surrounding temporary seismograph deployments. The labelled stations are mentioned in the main text. The star denotes permanent seismograph station LSZ. The arrows denote absolute plate motion (APM) direction in a no-net-rotation frame (Kreemer *et al.* 2014). Green and blue lines show individual and stacked splitting parameters, respectively, measured in previous shear-wave splitting studies (Barruol & Ismail 2001; Bagley & Nyblade 2013; Reed *et al.* 2017; Elsheikh 2019).

the Lufilian orogeny is unique among Africa's Pan-African belts, and records several orthogonal deformational fabrics at uppermost-crustal depths (e.g. Porada & Berhorst 2000; Key *et al.* 2001) which have made it difficult to piece together a coherent picture of the region's tectonic evolution.

Plate-scale tectonic processes, such as the development of orogenic belts, should be manifested as a fossil anisotropic fabric preserved within the lithosphere via the development of lattice preferred orientation (LPO) in mantle minerals such as olivine (e.g. Zhang & Karato 1995). SKS splitting studies from other late Phanerozoic and Precambrian orogenic belts, such as the Caledonian and Trans-Hudson orogenies (e.g., Bastow *et al.* 2007; Gilligan *et al.* 2016), find olivine LPO tends to parallel the strike of these belts if deformation simultaneously affected both the crust and lithospheric mantle. However, the historical lack of high-resolution deep-penetrating geophysical constraints on lithospheric structure across the Central African Plateau has so-far limited tectonic interpretations to upper-crustal depths. Whether or not surface faulting is related to thin-skinned, 'crustal' events, or processes that also affected the lithospheric mantle, remain poorly understood.

Large-scale shear zones and granitic intrusions, such as the Mwembeshi shear zone and Hook Granite (Fig. 1a), respectively, are also associated with the latest stages of the Pan-African orogeny (~550–530 Ma; e.g. de Swardt *et al.* 1965; Naydenov *et al.* 2014). Some studies hypothesize the Mwembeshi shear zone to be a major continental-scale feature, possibly a Proterozoic suture zone (e.g. John & Schenk 2003), that has accommodated significant amounts of oblique, dextral, and most recently, sinistral shearing (e.g. de

Swardt *et al.* 1965; Daly 1988). Magnetotelluric imaging across the Luangwa Rift Valley illuminates a conductive discontinuity at mantle lithospheric depths that is interpreted by Sarafian *et al.* (2018) to be the Mwembeshi shear zone, whose weakness allowed the localization of the Luangwa Rift Zone during Permo-Triassic Karoo rifting. Other geochronological studies across the Mwembeshi shear zone and juxtaposed Hook intrusion in central Zambia, however, find little evidence for significant plate-scale shearing (Naydenov *et al.* 2014). Thus, whether or not the shear zone is a thin-skinned crustal-scale feature resulting from intraplate deformation during the Pan-African orogeny, or the plate-scale remnant of Precambrian suture zones, remains enigmatic.

To address these research questions, we conduct a shear-wave splitting study of seismic anisotropy using SKS, SKKS, and PKS phases (hereby collectively referred to as XKS) recorded by 73 seismograph stations across the Central African Plateau (Fig. 1b). When an XKS wave traverses an anisotropic medium, it splits into two orthogonally polarized waves, one travelling faster than the other. The azimuth (ϕ) of the fast polarization direction, and the delay time (δt) between the fast and slow arrivals at a seismograph station, constitute 'splitting parameters' that provide a simple means to characterize the direction and strength of anisotropy (e.g. Silver & Chan 1991). In our analysis, we use data from the new Copper Basin Exploration Science (CuBES) seismograph network (Fig. 1b), which was designed to traverse the region's scarcely explored tectonic units in central Zambia, as well as existing surrounding networks. Shear-wave splitting allows us to assess lithospheric deformation fabrics associated with both past

and present tectonic events, revealing insights into the orientation, significance and depth extent of various phases of deformation. Also explored is whether more recent episodes of deformation, such as Permo-Triassic Karoo rifting, have overprinted older plate-scale fabrics. The impact of asthenospheric mantle flow, whether related to the African Superplume or Africa's absolute plate motion, on the splitting results is also assessed.

2 TECTONIC BACKGROUND

The Central African Plateau (Fig. 1a) spans 2 Ga of Earth history, from Archean cores to a series of Precambrian-Paleozoic collisions, culminating in the so-called Pan-African orogeny. The region's pre-Pan-African lithosphere comprises numerous cratons—the Archean Congo and Kalahari Cratons, and Proterozoic Bangweulu Craton—and flanking Paleo-and-Mesoproterozoic orogenic belts (~ 2.1 – 0.9 Ga) within which subsequent rifting and collisional episodes were able to develop (e.g. Daly 1986; Fritz *et al.* 2013).

2.1 The Pan-African Lufilian and Zambezi belts

Today, the majority of the Central African Plateau is composed of two mobile belts that formed during the Pan-African assembly of Gondwana which featured the collision of the Congo and Kalahari Cratons (~ 650 – 530 Ma; Fig. 1a): the Lufilian Arc and Zambezi Belts (Fig. 1a; e.g. Hanson *et al.* 1994; Porada & Berhorst 2000; John *et al.* 2004). Prior to orogeny, both regions were characterized by continental rift/ocean basin settings developed during the break-up of the Rodinia supercontinent (e.g. Porada & Berhorst 2000; John & Schenk 2003). The Lufilian Arc marked the location of the wide Neoproterozoic Katangan Basin (~ 880 – 820 Ma; e.g. Hanson *et al.* 1994; Porada & Berhorst 2000) which evolved into a passive continental margin setting with 7–10 km of basin infill (e.g. Kampunzu & Cailteux 1999; Kipata *et al.* 2013). The Arc is broadly divided into five tectonic regions (Fig. 1a): (I) the External Fold and Thrust Belt of dominantly NW-to-NE-vergent thin-skinned thrusting; (II) the Domes Region is thought to represent the central rift axis during Katangan basin formation and subsequent locus of greatest compression during the Pan-African orogeny, as evidenced by the exposure of Proterozoic basement rock, high-grade metamorphism and presence of early-stage-rift tholeiitic magmatism (e.g. Kampunzu & Cailteux 1999; Porada & Berhorst 2000); (III) the Synclinorial Belt and (IV) the Katanga High represent the lower-metamorphic grade regions of the arc, however, the boundary between the two is uncertain. Porada & Berhorst (2000) proposed the Katanga High may have been the northern margin of the overriding plate during collision; (V) the Katangan Aulacogen represents the foreland basin. The Lufilian Arc's arcuate nature is unique across Africa's orogenic belts. Hypotheses for the cause of this shape include the presence of an indenter in the south (e.g. Unrug 1983), clockwise microplate rotation (e.g. Kampunzu & Cailteux 1999), or simply a consequence of the regional stress field that may have been composed of two separate, orthogonal phases of shortening (E–W and NW–SE; e.g. Key *et al.* 2001; Kipata *et al.* 2013; Naydenov *et al.* 2014).

In the south, the Pan-African Zambezi Belt (Fig. 1a) is thought to mark a suture zone resulting from the closure of a Neoproterozoic intracratonic basin (Hanson *et al.* 1994) or the subduction of a major ocean ~ 650 Ma (e.g. Hanson *et al.* 1988; John & Schenk 2003), preserving evidence of this process in the form of high-temperature high-pressure eclogitization of gabbroic rocks (Fig. 1; e.g. Cosi *et al.* 1992; John & Schenk 2003). South of the Zambezi Belt, lies the Choma–Kalomo Block which is thought to be a re-worked portion of the neighbouring Kalahari/Zimbabwe Craton, however, there is

thus far no definitive evidence for Archean-age crust (e.g. Glynn *et al.* 2017).

2.2 The Mwembeshi shear zone

Separating the Lufilian and Zambezi branches of the Pan-African orogeny, is the Mwembeshi shear zone (Fig. 1a) which was last active in early Paleozoic times (~ 520 Ma). The shear zone's tectonic evolution is poorly known but it is assumed to be a plate-scale sinistral shear zone that experienced up to 200 km of horizontal displacement (e.g. de Swardt *et al.* 1965; Unrug 1983) during the Pan-African convergence of the Kalahari and Congo Cratons. Alternative models propose the Mwembeshi shear zone was once a suture zone in Proterozoic times, experiencing several phases of reactivation, including reverse and dextral transform motion, prior to its latest sinistral phase (Coward & Daly 1984; Daly 1988; Porada & Berhorst 2000). Juxtaposed immediately to the north of the shear zone, is one of the largest magmatic complexes across the region—the Hook granitic batholith—which was emplaced ~ 550 – 530 Ma (e.g. Naydenov *et al.* 2014) within the innermost, low-metamorphic grade section of the Lufilian Arc (Fig. 1a; e.g. de Swardt *et al.* 1965).

2.3 Mesozoic–recent rifting

Subsequently, Karoo rifting developed during the break-up of Gondwana in the Permo-Triassic period (~ 250 Ma) forming several rift valleys across central Africa (e.g. Catuneanu *et al.* 2005), most notably the Luangwa, Kafue and Zambezi Rifts (Fig. 1a). The most extensive of these is the Luangwa Rift zone which is thought to have developed in weakened lithosphere along the Mwembeshi shear zone (e.g. Sarafian *et al.* 2018) and may have been reactivated in the Pliocene by the same stress field responsible for the Cenozoic East African Rift System, accommodating 0.4 – 0.6 mm yr $^{-1}$ of plate motion (e.g. Wedmore *et al.* 2022). Nascent rifting related to the southwestern branch of East African Rift System, has also developed across the broader Central African Plateau in Pliocene times, as evidenced by the occurrence of Kimberlites in Zone V of the Lufilian Arc (Batumike *et al.* 2008) and moderate seismicity across the Plateau (Fig. 1a; e.g. Delvaux & Barth 2010; Craig *et al.* 2011), and may geodynamically link to the Pleistocene Okavango Rift in Botswana (e.g. Daly *et al.* 2020).

3 SEISMIC ANISOTROPY AND XKS SPLITTING ANALYSIS

Seismic anisotropy refers to the directional dependence of seismic wave speed, often assessed through shear-wave splitting. SKS, SKKS and PKS phases (collectively referred to as XKS) are ideally suited for shear-wave splitting studies since they are P-to-S converted phases radially polarized at the core–mantle boundary, thus preserving no source-side anisotropy. Plate-scale deformation can lead to the development of an anisotropic fabric within the lithosphere through the alignment of olivine crystals—the most abundant mineral in the Earth's upper mantle. When olivine is deformed in response to shear strain, an LPO may develop, with its *a*-axis aligned parallel to the direction of flow or shear-strain (e.g. Zhang & Karato 1995; Tommasi *et al.* 2000). Thus, measurements of seismic anisotropy are powerful ways to map density driven asthenospheric flow, absolute plate motion directions (e.g. Debayle & Ricard 2013), or lithospheric deformation from both past and ongoing tectonic processes (e.g. Silver & Chan 1991; Silver 1996; Savage 1999; Kendall *et al.* 2006).

Our teleseismic data set comes from 35 temporary broad-band seismograph stations deployed during the CuBES project (Fig. 1b).

The network consisted of Gürulp CMG-3T, CMG-ESP and CMG-6TD instruments, with a natural period of 120 s, and recorded data at 100 Hz between 2022 May and 2023 November (see Table S1 in the supplementary material for further station details). Additional data come from IU network permanent station LSZ in Lusaka (Albuquerque Seismological Laboratory/U. S. Geological Survey 2014), operational since 1994, and from several temporary deployments that operated at various periods between 2006 and 2023: the ZP (Nyblade 2007) and AF AfricaArray seismic networks (Penn State University 2004), BX Botswana seismic network (Botswana Geoscience Institute 2001) and XK SAFARI seismic network (Fig. 1b; Gao *et al.* 2012). Visual inspection of magnitude >5.5 earthquakes at epicentral distances $>88^\circ$ from each seismograph station yielded a data base of 2627 high signal-to-noise ratio XKS-phase earthquake-station pairs, suitable for shear-wave splitting analysis, of which 493 were incorporated into the final data set. The analysis avoids direct S-wave arrivals because of associated problems such as source-side splitting and D'' grazing phases. Data were filtered prior to analysis with a zero-phase two-pole Butterworth bandpass filter with corner frequencies of 0.04–0.3 Hz.

XKS splitting analysis was conducted using the semi-automated approach of Teanby *et al.* (2004), based on the methodology of Silver & Chan (1991), with errors estimated using the method of Walsh *et al.* (2013). Elliptical particle motion and energy on the tangential component seismogram are evidence of shear-wave splitting. Horizontal component seismograms are rotated and time

shifted to minimize the second eigenvalue of the covariance matrix for particle motion for 100 different time windows around the shear-wave arrival. This is equivalent to linearizing the particle motion and reducing the tangential component energy. If the particle motion is linearized initially, this corresponds to a ‘null’ measurement and indicates that the anisotropic fast direction is either parallel or perpendicular to the waveform backazimuth, no anisotropic medium is present, or that multiple layers of contrasting anisotropy appear isotropic as a whole. Good null results are selected only when a high signal-to-noise ratio is visible on the radial component and energy on the transverse component is lacking from visual inspections. Cluster analysis is then used to find the most stable splitting parameters across the entire range of window lengths. The final choice of shear-wave analysis window corresponds to the measurement with the lowest error in the cluster with the lowest variance (Teanby *et al.* 2004). An example of a high-quality splitting measurement is shown in Fig. 2. Only measurements where the difference between the backazimuth and source polarization direction of the XKS phase is $\lesssim 15^\circ$ are accepted, thus avoiding spurious results that could be associated with core–mantle boundary topography and SKS multipathing due to large lateral wave speed variations in the lowermost mantle (e.g. Restivo & Helffrich 2006; Ward *et al.* 2020). Additional quality control was enforced by visual inspection of each result to ensure linearization of the particle motion, and by employing strict upper limits on ϕ and δt estimates of $\pm 20^\circ$ and ± 0.3 s, respectively. We typically obtained between two and ten

Network: Z1 Station: Z31K Event: 2022-09-17 13:41:17 (23.09°N, 121.44°E, depth=10.0 km) BAZ: 68.85° Δ: 100.04°

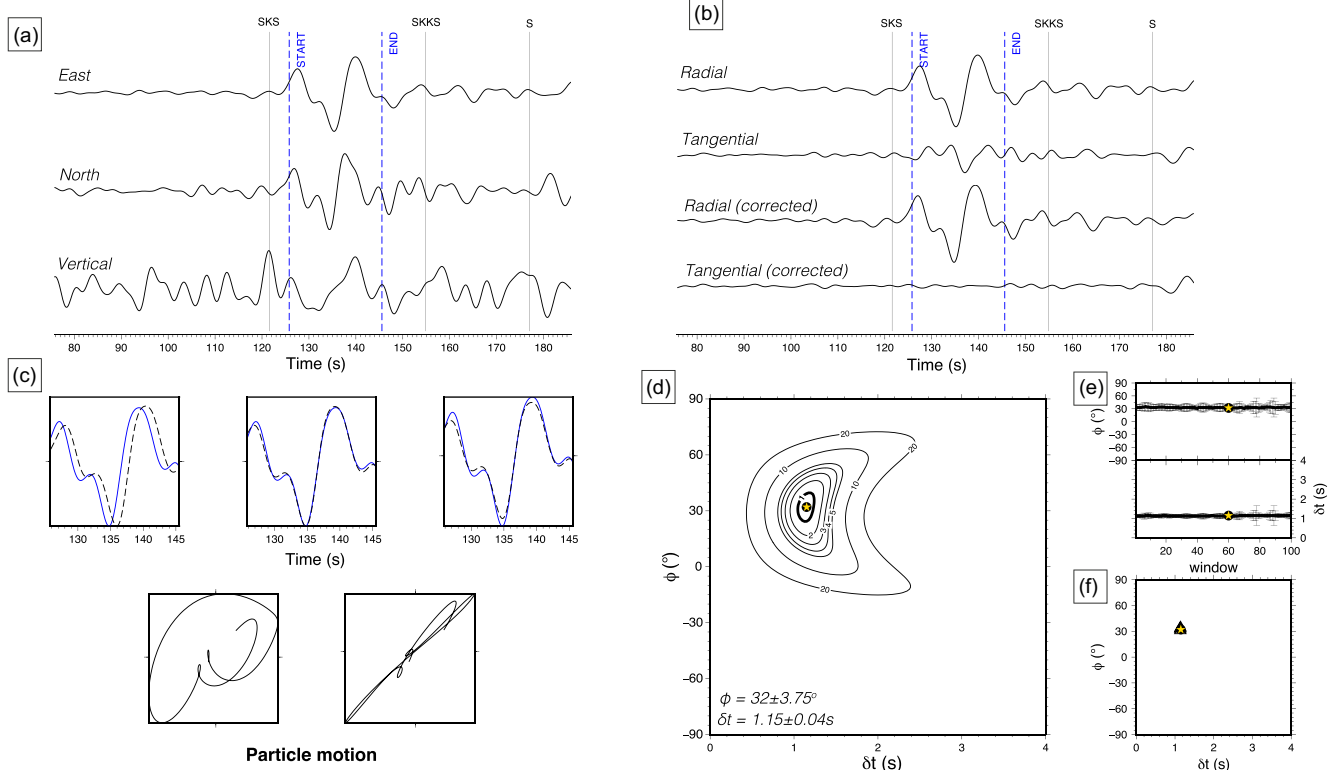


Figure 2. Example of a high-quality shear-wave splitting result: (a) the original filtered waveforms, with the final window start and end points marked, as well as predicted SKS, SKKS and S arrival times; (b) the rotated waveforms, before and after correction for splitting; (c: top row) the calculated fast (solid blue) and slow (dashed) waves, first amplitude-normalized at their original time points (left), then amplitude-normalized and time-shifted by δt (middle), then original amplitude and time-shifted by δt (right); shown below are the original particle motion (left), and linearized particle motion after correction (right); (d) error surface for calculated result; (e) splitting parameters for each window analysed, where the yellow star indicates the accepted window; (f) cluster analysis results for ϕ and δt from all 100 windows. The values are stable across the full range of windows.

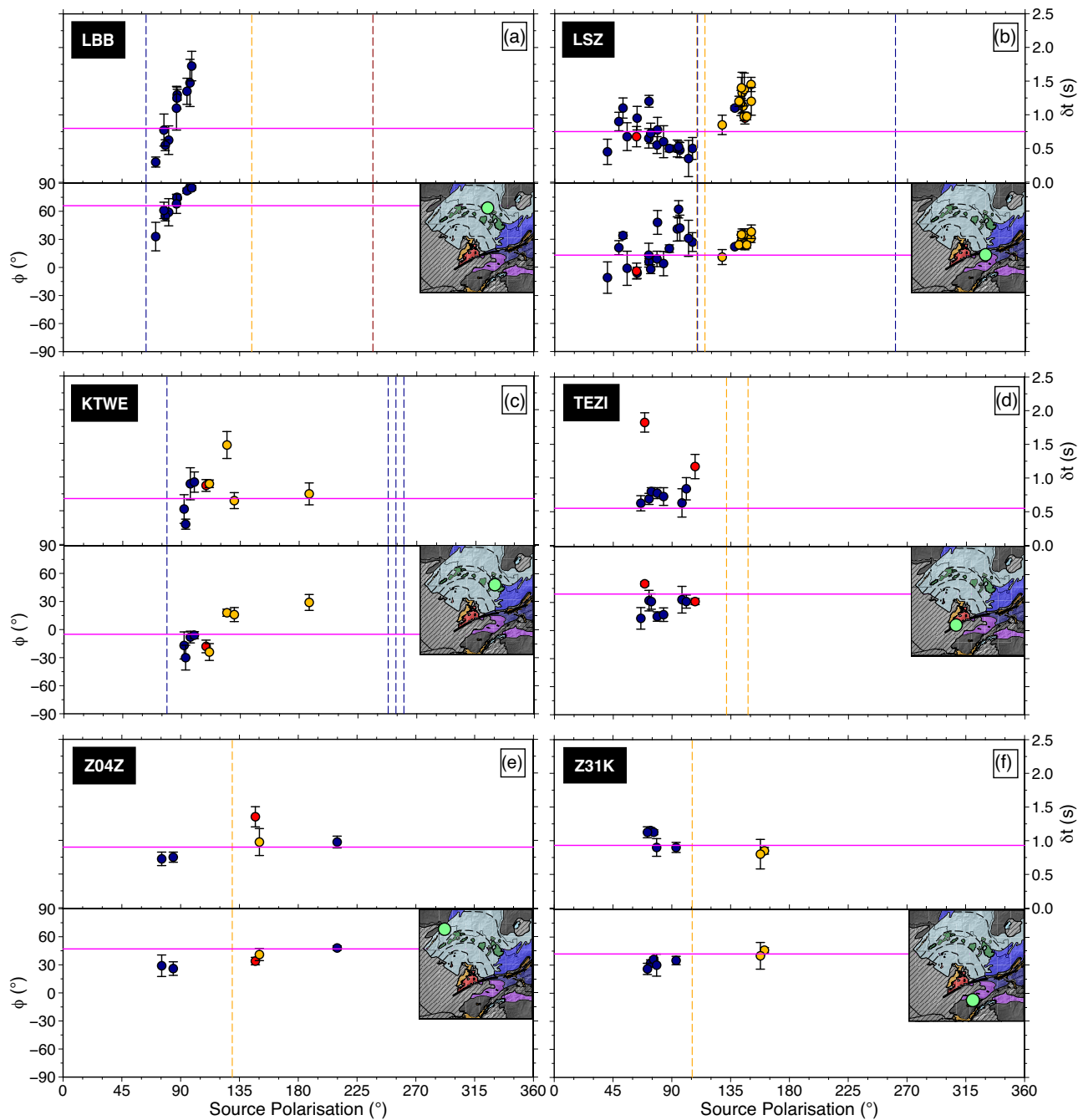


Figure 3. The distribution of splitting parameters plotted against the source polarization of the incoming wave at various stations. (a) Station LBB, located north of the Domes region in the Lufilian Arc. (b) Permanent station LSZ in the Zambezi Belt. (c) Station KTWE, located within the Domes region. (d) Station TEZI along the Mwembeshi shear zone. (e) CuBES network station Z04Z at the edge of the Congo Craton. (f) CuBES network station Z31K on the Choma-Kalamo Block. The station locations are each shown by a green circle in the inset tectonic map. Blue, red and yellow results correspond to SKS, SKKS and PKS phases, respectively. The vertical dashed lines are null measurements, coloured by phase. The horizontal magenta lines indicate the values of ϕ and δ_t obtained by the stacking procedure. Error bars show the 95 per cent confidence interval on each measurement. At most stations we only obtain results from earthquakes in a limited backazimuth range. See [supplementary material](#) for a full set of plots for the remaining stations ([Figure S1](#)).

good quality splitting measurements per station. A list of accepted earthquakes for each station is given in the [supplementary material](#) ([Table S4](#)).

To obtain a single pair of splitting parameters at stations where good quality individual measurements were obtained, we adopt the stacking procedure of Restivo & Helffrich (1999). In the stack, increased weighting is assigned to higher signal-to-noise ratio results, allowing them to exert greater control on the determined splitting

parameters. Stacking results at each station implicitly imposes the assumption of a single, horizontal, homogeneous anisotropic layer. Where this assumption is invalid, we expect to see splitting parameters that vary according to the backazimuth of the incoming shear wave (Fig. 3). For example, characteristic of a two layer anisotropic model, is a 90° periodicity or large peak-to-peak variation in splitting parameters (e.g. Silver & Savage 1994). Where a dipping principle anisotropic axis exists, ϕ variations with backazimuth are

also expected, although not as sharp as those in a multiple layer scenario (e.g. Liddell *et al.* 2017).

4 RESULTS

Accepted splits were recorded at 68 of the 73 stations analysed, and are comprised of 215 SKS, 110 PKS and 33 SKKS arrivals (Fig. 4a). Most splits across the network have $0.4 \text{ s} < \delta t < 2.0 \text{ s}$. We recorded 135 null results across 52 stations. Null measurements have an inherent 90° ambiguity in ϕ , and are thus reported as pink crosses in Fig. 4a. For most stations, we found no significant variation in ϕ or δt as a function of backazimuth (Fig. 3 and supplementary material Figure S1); our backazimuthal earthquake coverage at most stations is unfortunately insufficient to resolve more complex dipping or multilayer patterns of anisotropy (Fig. 3). However, variations in ϕ and δt at some stations (e.g. LBB, KTWE, LSZ) suggest more complex patterns and the potential for dipping and/or multilayer anisotropy (Fig. 3). At station LBB, abrupt changes in ϕ and δt over very short ($< 20^\circ$) backazimuth ranges would be diagnostic of a two layer model, rather than a one with a single dipping layer (e.g. Liddell *et al.* 2017). Tables S2 and S3 in the supplementary material contain a list of all the final splitting measurements, stacked results and associated uncertainties determined for each station.

4.1 Anisotropic layer thickness

The value of δt is a function of the thickness and strength of the anisotropic medium. Average δt varies throughout the region from $\delta t > 1.2 \text{ s}$ in southeastern Zambia to $\delta t < 0.7 \text{ s}$ across the northwestern parts of the Lufilian Arc (Fig. 4b), indicating that there are changes in the strength and/or anisotropic layer thickness across Zambia. For a shear-wave travelling vertically through a single layer of constant isotropic shear-wave velocity (β_0), the layer thickness (L) can be approximated using $L = \delta t \beta_0 / K$, where δt is the SKS splitting delay time and K is the percentage anisotropy. Assuming an average upper mantle velocity of 4.48 km s^{-1} (Kennett *et al.* 1995) and 4 per cent anisotropy (e.g. Tommasi *et al.* 2000), a δt of 1.4 s requires a 170-km-thick anisotropic medium. Given average lithospheric thickness across the region is greater than 150 km (Figs 5c and d; Priestley *et al.* 2018; Emry *et al.* 2019), the majority of the anisotropic signal may be sufficiently explained by structures in the lithosphere. Thicker anisotropic layers would be possible if two or more layers of different orientation interact subtractively.

5 DISCUSSION

5.1 Causes of observed anisotropy

Across the study area, we commonly observe $\delta t > 1 \text{ s}$, implying a mantle contribution to the anisotropy: while some crustal minerals, such as amphibolite (e.g. Ko & Jung 2015; Liu & Cao 2023), are highly anisotropic, the amount of splitting associated with normal, $<45\text{-km-thick}$, continental crust (e.g. Kachingwe *et al.* 2015; Ogden *et al.* 2022) is relatively small ($\delta t < 0.5 \text{ s}$ of the total delay time; Barruol & Mainprice 1993; Silver 1996). APM of the African Plate has been a relatively constant $\sim 29 \text{ mm yr}^{-1}$ over the past 30 Ma, and is below the $\sim 40 \text{ mm yr}^{-1}$ minimum required for notable basal drag fabric development (e.g. Debayle & Ricard 2013). Density driven

mantle flow related to African superplume material (e.g. Forte *et al.* 2010) at uppermost mantle depths is also likely to be small below the network—plume-related slow wavespeeds are constrained to below mantle transition zone depths in this region (e.g. Hansen *et al.* 2012; Boyce *et al.* 2021). APM-induced asthenospheric fabrics or density-driven mantle flow are expected to produce smooth variations in splitting parameters across the network, a consequence of Fresnel zone arguments (length-scales $\sim 150 \text{ km}$; e.g. Alsina & Snieder 1995). Instead we observe no consistent network-wide alignment of ϕ with APM or flow from the African Superplume. Short length-scale variations ($< 100 \text{ km}$) in ϕ and δt , where a relatively thick lithosphere ($> 150 \text{ km}$; Fig. 5d) is imaged in surface-wave tomography (Priestley *et al.* 2018; Afonso *et al.* 2022), imply a fossil lithospheric fabric is likely the dominant cause of the observed anisotropy. We therefore reject APM and flow of superplume material as the dominant cause of our observed anisotropy, as opposed to Bagley & Nyblade (2013) and Reed *et al.* (2017). However, in the absence of detailed lithospheric thickness measurements across the region, we cannot preclude some effect of rheological channelling of flow at base-of-the-lithosphere topography (e.g. Ebinger & Sleep 1998; Sleep *et al.* 2002).

Observations of anisotropy attributed to the D'' discontinuity and African Large Low Shear-Wave Velocity Province have also been made below southern Africa (e.g. Reiss *et al.* 2019; Ward *et al.* 2020), based on discrepant SKS and SKKS splitting observations for the same earthquake-station pairs. Where both SKS and SKKS measurements exist for the same earthquake-station waveforms across our network, splitting parameters are similar. Additionally, waveforms with observed differences ($< 15^\circ$) between the backazimuth and source polarization—often thought to be a consequence of anisotropy related to lowermost mantle anomalies (e.g. Restivo & Helffrich 2006; Ward *et al.* 2020)—have been removed from the data set.

The lack of active tectonics since Permo-Triassic Karoo rifting in parts of the Central African Plateau (~ 250 – 200 Ma) further rules out active melt in the lithosphere as a possible cause. The southwestern branch of the Cenozoic East African Rift System has only very recently extended into Zambia—the absence of Quaternary volcanism and the presence of deep seismicity focused along major fault structures (e.g. Craig *et al.* 2011; Daly *et al.* 2020) indicates a predominantly mechanical present-day early-stage rift system, lacking the highly anisotropic melt-intrusions that are abundant in the East African Rift further north (Kendall *et al.* 2005; Ebinger *et al.* 2024). Our discussion therefore proceeds on the assumption that our data are primarily sensitive to fossil lithospheric fabrics across the region.

5.2 Comparison to previous studies

In areas where our results overlap with previous studies, the agreement between splitting measurements is largely very good (Figs 1b and 4). Previous SKS splitting studies in central and southern Africa have attributed the observed anisotropy to various causes: APM-induced mantle flow (e.g. Reed *et al.* 2017; Andriampanomanana *et al.* 2024), the flow of African Superplume material (Bagley & Nyblade 2013), and preserved lithospheric fabrics in cratonic regions and orogenic belts (e.g. Silver 1996; James & Fouch 2002). Barruol & Mainprice (1993) measured complex splitting parameters at permanent Geoscope seismograph stations across the African continent, including station LSZ, which they attribute to be primarily a signature of the regional cratonic and orogenic belt setting;

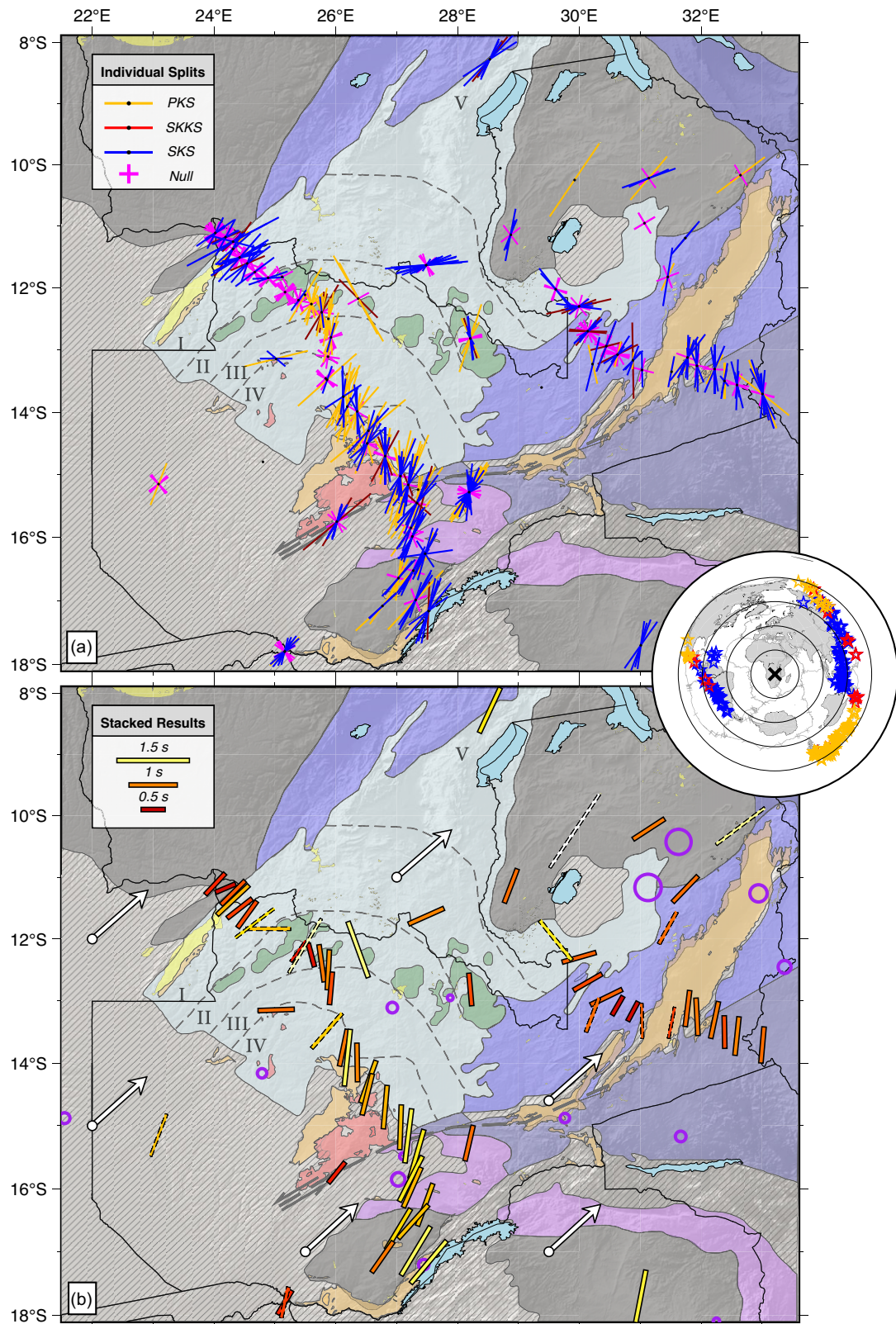


Figure 4. (a) All recorded splits and null measurements plotted against regional tectonic units. The orientation of the coloured lines represents the fast axis ϕ , and their length the delay time δt , of the anisotropy. Nulls are represented as pink crosses oriented parallel and perpendicular to the backazimuth of the recorded arrival. Right inset: earthquakes that yielded good quality splits and nulls, coloured by phase used. (b) Stacked splitting parameters plotted against regional tectonic units. The thinnest and medium-thickness bars with dashed outlines represent stations with only one and two accepted splits, respectively; the rest have three or more. White arrows show APM which is $\sim 29 \text{ mm yr}^{-1}$ (Kreemer *et al.* 2014). Purple circles indicate points where a change in azimuthal anisotropy is detected using Quasi Love waves from Merry & Eakin (2024). See Fig. 1 for a key to the geology.

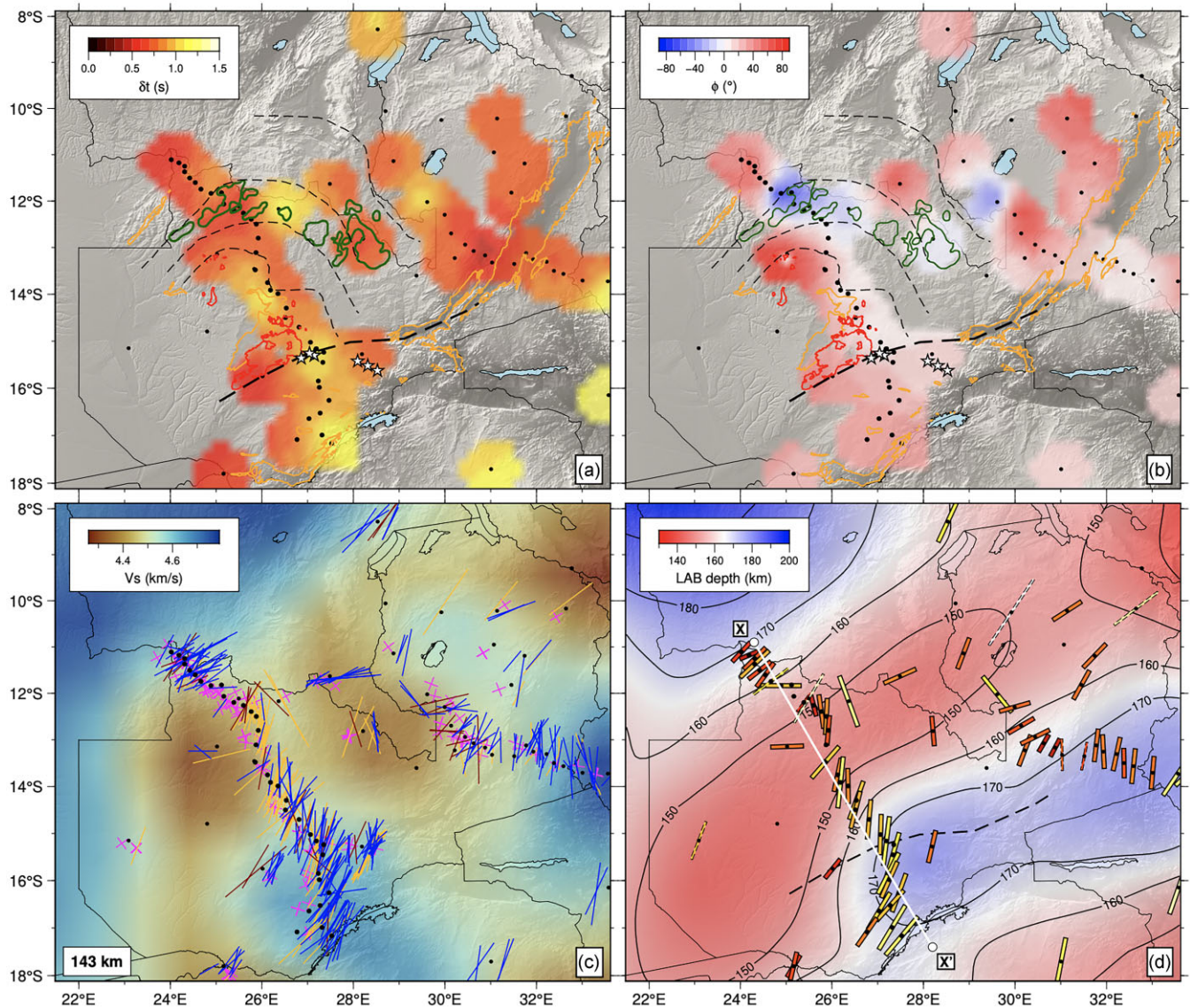


Figure 5. (a) Interpolated δt and (b) ϕ results across the region. Outlines of some of the key tectonic units are also shown: Karoo rifting (orange outline), the Domes region (green), Lufilian Arc subdivisions (thin dashed lines), Mwembeshi shear zone (thick dashed line), Hook granitic intrusions (red), eclogites (white stars). Seismograph stations are shown as dots. (c) Observed XKS splitting results projected on to their 150 km depth piercing point, against a depth slice from the continent-scale ambient noise tomography model of Emry *et al.* (2019). (d) Stacked splits plotted against the lithospheric thickness map of Priestley *et al.* (2018). X–X' shows the start and end points of the shear-wave splitting profile shown in Fig. 6.

they find little evidence for backazimuthal variation in splitting parameters at station LSZ, in agreement with our results. Using AF network stations, as far south as northern Zambia, Bagley & Nyblade (2013) postulate that the dominant NE anisotropic pattern is consistent with mantle flow from the African Superplume with some deviations around Archean cratonic lithosphere, such as the Bangweulu and Tanzanian Cratons. Our results generally corroborate the NE–SW oriented ϕ observed by Bagley & Nyblade (2013) for some stations within and to the north of the Bangweulu Craton (e.g. PWET and KASM). However, in stations further south, especially within the Domes and Lufilian Arc, abrupt changes in ϕ , including the presence of NW–SE fabrics which severely deviate from APM directions (e.g. KTWE, GABZ; Figs 4 and 5b), suggest a fossil lithospheric fabric source. More recently, Merry & Eakin (2024) found evidence of Quasi Love wave scattering—an indicator of changes in azimuthal anisotropy—in parts of the Lufilian Arc,

Zambezi belt and edge of the Bangweulu Craton (Fig. 4b), which are interpreted as fossilized lithospheric anisotropy contrasts.

Reed *et al.* (2017) reported splitting measurements across the Luangwa Rift Valley SAFARI seismic network (Fig. 1b) and attributed the spatial coherency and lack of parallelism with border faults to an asthenospheric, APM-induced, flow origin. An exception is splitting on the western flank of the Luangwa Rift, where ϕ parallels the rift axis. Our results generally agree with Reed *et al.* (2017), and while they do not strike parallel to rift border faults, short length-scale variations in thick lithosphere (~ 170 km) that generally matches the anisotropic layer thickness (see Section 4), hint at a substantial fossil lithospheric contribution: the approximately N–S ϕ directions also parallel the strike of Pan-African-related fabrics in the Irumide Belt west of the Luangwa Rift (e.g. Banks *et al.* 1995). Nevertheless, we cannot preclude a certain amount of asthenospheric influence.

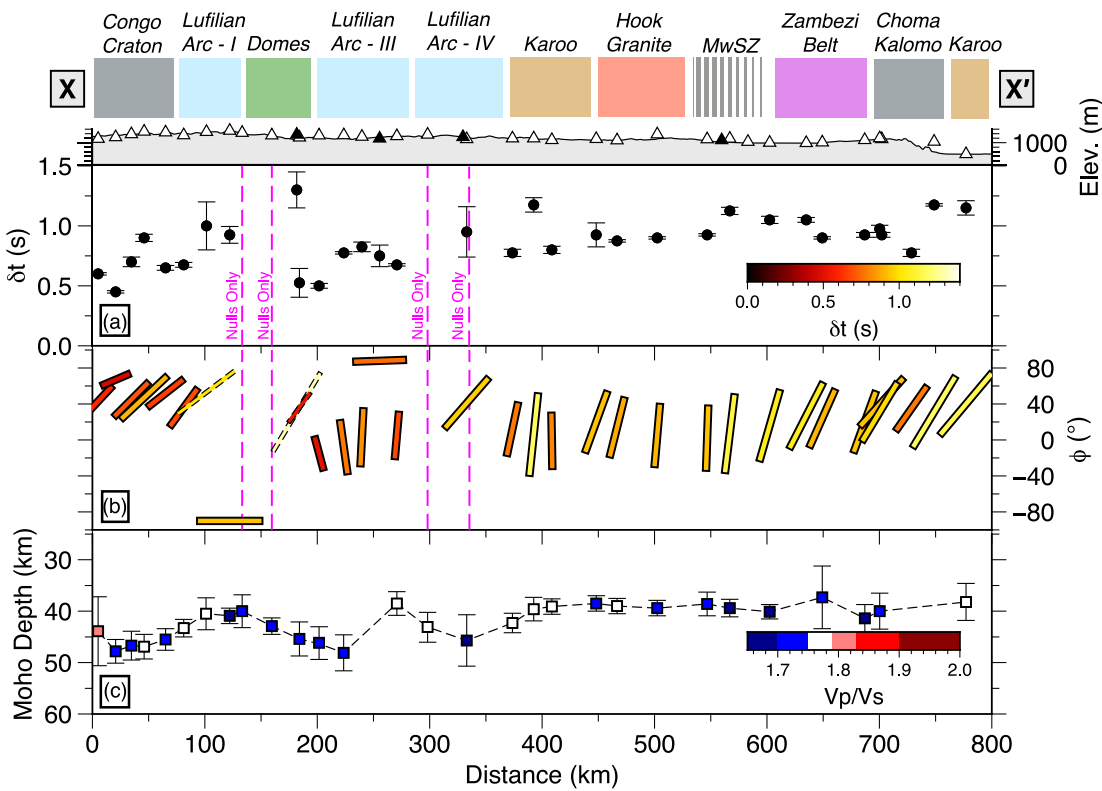


Figure 6. Profile of splitting results within 100 km of the ~750-km-long CuBES seismograph network. See Fig. 5d for the profile location. (a) δt and associated errors. Stations which only produced null measurements are shown by the vertical dashed lines. (b) Stacked XKS anisotropy ϕ axes with colour representing δt . Stacked results with a dashed outline contain less than two measurements. (c) Cross-section of crustal thickness and V_p/V_s ratio across the network from the H- κ receiver function study of Ogden *et al.* (2022). The broad tectonic subdivisions, as per Fig. 1 are shown above the profiles. White and black triangles on the topographic profile are projected CuBES and Africa Array network stations, respectively. MwSZ: Mwembeshi shear zone.

Next, we investigate the anisotropic patterns across central Zambia's Precambrian terranes and shear zones where seismograph deployments were previously sparse.

5.3 Deformation across the Mwembeshi shear zone

Major plate-scale strike-slip faults worldwide, both active and extinct, are generally associated with fault-parallel anisotropic fast directions (within 5–20° of the fault plane) due to coherent deformation in a lithospheric shear zone under a high-strain rate (e.g. Silver & Chan 1991; Barruol & Ismail 2001; Bastow *et al.* 2007; Vauchez *et al.* 2012; Reiss *et al.* 2016; Merry *et al.* 2021). However, stations within 100 km of the sinistral Mwembeshi shear zone, do not exhibit such fault-parallel ϕ , nor does the fault separate two regions of differing anisotropic characteristics (Figs 4, 5b and 6). Several hypotheses could explain these observations: the shear-zone may be too narrow at mantle depths, too thin-skinned, or lacking in sufficient fault-parallel displacement to have developed a shear-fabric that is discernible via XKS shear-wave splitting analysis. Our results thus corroborate the view from the structural and geochronological study of Naydenov *et al.* (2014) that the Mwembeshi shear zone is unlikely to be a significant continental-scale structure, at least not in central Zambia. An exception to this is AF network station TEZI in southern Zambia (Fig. 1), which has an average ϕ direction better aligned with the strike of the shear-zone (within 20°). Further north, along the northward continuation of the shear zone, at the eastern flank of the Luangwa Rift Valley, magnetotelluric imaging (Sarafian *et al.* 2018) has revealed a conductive discontinuity

to mantle lithospheric depths, whose weakness may have allowed for the localization of strain during Luangwa Rift-development. In this region, we find some fault-parallel ϕ , however, this may only be coincidental given the consistency of ϕ with the approximately N–S/NW–SE orogenic fossil fabrics recorded in neighbouring tectonic units (e.g. the Irumide Belt; Fig. 4). If rifting in Luangwa was accompanied by dike intrusion during Karoo rifting then that might also explain the rift-parallel ϕ (e.g. Kendall *et al.* 2005, 2006).

If the Mwembeshi shear zone is a plate-scale feature, then an alternative explanation for a lack of fault-related ϕ is strain that is too low for strong LPO to have formed during its latest active phase as a sinistral strike-slip fault. Laboratory experiments that generate olivine LPO under simple shear strain at simulated upper mantle conditions indicate that shear-plane parallel fast directions are expected only at total shear strain $\gamma > 1.1$ (Zhang & Karato 1995) across the fault. For $\gamma < 1.1$, ϕ is expected to be intermediate between fault strike and ϵ_1 (axis of minimum compressive stress), and would appear clockwise in left-lateral faults, and counter-clockwise in right-lateral faults.

To examine whether total shear strain during the Mwembeshi shear zone's active phase was enough to accrue shear-zone parallel ϕ , we use the relationship $\gamma = x/W$, where x is offset assuming distributed simple shear and W is mantle shear zone width. In the absence of detailed structural constraints, displacement along the Mwembeshi shear zone has been assumed to be of the order 100–200 km considering its role in the regional tectonics (e.g. de Swardt *et al.* 1965). To accommodate $x \approx 150$ km of displacement, and

maintain a low total shear strain of $\gamma < 1.1$, the width of the shear-zone in the mantle would have to have been greater than 136 km—more localized, and shear-plane-parallelism may have been achieved given this amount of displacement. If shear-zone width was indeed narrower, then displacement is unlikely to have been significant, unless the mantle shear zone was sufficiently narrow (< 50 km from Fresnel zone arguments; Alsina & Snieder 1995) that it is not resolvable in our shear-wave splitting study. There is a marginal increase in δt across the fault zone in central Zambia which may indicate a broad zone of increased deformation, however this increased δt pattern spans a region much wider (~ 300 km) than the fault itself and may instead be the result of co-aligned fossil lithospheric fabrics and sublithospheric mantle flow. Due to insufficient backazimuthal coverage, we cannot resolve definitively if multiple anisotropic layers exist. Given that the Mwembeshi shear zone may have formed in the remnants of Neoproterozoic suture zones (e.g. Coward & Daly 1984; Daly 1988; John & Schenk 2003), we also cannot preclude the possibility that some impression remains on LPO fabrics from strain localization that occurred prior to the development of sinistral shearing.

5.4 Evidence for complex anisotropy in the Lufilian arc

A striking observation in our results is the lack of coherent anisotropic fabrics across the Pan-African Lufilian Arc that are difficult to attribute to a single uniform episode of deformation (Figs 4): NE–SW, N–S and NW–SE ϕ directions exist at very short length-scales (< 100 km). Nevertheless, changes in anisotropy appear to broadly correlate with the subprovinces of the Lufilian Arc (Figs 1a and 4b). In the western arm of the arc (I; Fig. 4), NE–SW directed anisotropy parallels mapped thrust and fold belts in the region, supporting the presence of NW–SE-directed compression that penetrated the lithosphere during the initial stages of orogeny (e.g. Kampunzu & Cailteux 1999; Porada & Berhorst 2000; Key *et al.* 2001; Eglinger *et al.* 2016). This pattern disappears in the Domes region (II; Figs 4 and 6) where surprisingly low δt and null measurements prevail (Figs 4 and 5a). However, where splitting is observed at stations in close proximity to the Domes, relatively large δt and NNW–SSE/NW–SE ϕ directions are observed, in stark contrast to the majority of the network (Figs 4, 5a and 5b).

Continental lithosphere is seldom isotropic, instead the prevalence of nulls near the Domes region (II) is best explained by the negative interaction of multiple anisotropic layers of orthogonal fast orientations or the influence of a complex dipping layer. Evidence for backazimuthal variations in splitting parameters, that may signify multiple layers, exists near the Domes region, at stations LBB and KTWE (Fig. 3), albeit in a short backazimuthal range not sufficient enough to warrant additional modelling. The Domes region may thus mark the junction between two distinct tectonic blocks that experienced intense re-working during the Pan-African orogeny (Fig. 6c). This is corroborated by the exposures of Paleoproterozoic granitic basement in conjunction with higher-grade metamorphism compared to the rest of the Lufilian Arc (e.g. Porada & Berhorst 2000). The presence of a deep and highly variable Moho topography and generally low Vp/Vs ratios (Ogden *et al.* 2022) also signify intense crustal shortening/re-working near the Domes region, the edges of which seem to coincide with stations that only recorded null measurements (Fig. 6c). Nulls and low δt observations are also often attributed to vertical or toroidal mantle flow from small-scale convection operating near the edge of a craton (e.g. De Plaen *et al.* 2014; Diaz & Gallart 2014). However, there is little evidence for a sharp lithospheric thickness step required to

induce small-scale convection or entrainment of mantle flow around a cratonic-root, in surface-wave-derived lithospheric thickness maps of the broader region (Fig. 5d; e.g. Priestley *et al.* 2018; Afonso *et al.* 2022).

The two inner Lufilian Arc zones, the Synclinorial Belt (III) and Katangan High (IV), are each associated with distinct anisotropic fabrics (Fig. 4b). In zone III, consistently low δt and N–S-trending ϕ is observed, whereas the Katangan High is characterized by higher δt and NNE–SSW-trending ϕ (Figs 4b and 6). The N–S anisotropic fabric is consistent with E–W shortening, matching the principle horizontal stress directions determined from structural geology studies that postulate an E–W Pan-African compressional phase postdates the initial NW–SE-trending fabric (e.g. Key *et al.* 2001; Kipata *et al.* 2013; Naydenov *et al.* 2014). Splitting delay times of $\delta t > 1$ s point towards plate-scale deformation, coherent in the crust and lithospheric mantle (e.g. Silver & Chan 1991). Low δt in the Synclinorial Belt may therefore signify thin-skinned tectonics that have failed to become well-established at mantle lithospheric depths or to completely overprint pre-existing fabrics relating to Neoproterozoic Katangan Basin development. The larger δt in the Katangan High may indicate greater lithospheric-scale fabrics, consistent with the view that this region may have delimited the northern margin of the overriding plate during the Pan-African orogeny (e.g. Porada & Berhorst 2000). Voluminous granitic magmatism also differentiates this region from the rest of the Lufilian Arc, and may have also imprinted a large δt fabric in the region. Where Karoo rifting has been mapped in surface-geology, short-length-scale deviations in ϕ also seem to correlate (Fig. 4b).

That a uniform anisotropic fabric is not evident in our shear-wave splitting study attests to the complex Pan-African processes that have shaped the Lufilian Arc. Abrupt variations in anisotropy indicate the absence of a single prevailing episode of lithospheric deformation. Where splitting variations attributable to fossil lithospheric fabrics are most dramatic—in the Domes region—the most intense re-working likely took place during the Pan-African orogeny (~ 520 – 500 Ma). During their early-Paleozoic development, these complex anisotropic zones may have manifest as fault and fracture networks facilitating fluid migration that ultimately led to the region's synchronous copper-rich mineralization.

5.5 Anisotropic signature of cratonic regions

Debate exists as to the nature and extent of the southeastern Congo Craton margin at lithospheric depths below the Central African Plateau. Archean rocks are only exposed on the surface below station Z01J (e.g. Thieme & Johnson 1981), however some studies propose cratonic lithosphere extends below the Lufilian Arc region, as far south as the Mwunilunga fault in northwest Zambia (i.e. below station Z06N; Fig. 1b; Rainaud *et al.* 2003). The similarity of XKS measurements from station Z01J, which lies on Archean basement, to station Z06N, both in ϕ (NE-oriented) and δt (0.3–0.8 s), suggest the craton boundary at greater lithospheric depths may extend as far south as station Z06N below Zone I of the Lufilian Arc, south of which results become more variable (Fig. 4b). Alternatively, the consistent anisotropy could simply be related to the northwestern extent of the Lufilian Arc, with low δt suggestive of thin-skinned Pan-African collisional faulting.

Intriguingly, the Congo Craton margin, despite being a region of thick lithosphere (180–200 km; Fig. 5d), exhibits relatively weak anisotropy in our study ($\delta t \approx 0.3$ – 0.8 s). Weak-to-moderate azimuthal anisotropy is characteristic of many Archean cratonic regions worldwide, including the Tanaznia and Kaapvaal Cratons

in central and southern Africa, respectively (e.g. James & Fouch 2002; Fouch & Rondenay 2006; Chen & Niu 2016; Ebinger *et al.* 2024), suggesting a weak horizontal alignment of olivine at mantle lithospheric depths. Several tomographic models, however, instead observe a pervasive layer of large radial anisotropy, which is ubiquitous in many cratons globally (e.g. Lekić & Romanowicz 2011; Priestley *et al.* 2020; Boyce *et al.* 2024). Most recently, using a joint inversion of Love and Rayleigh wave dispersion data, Boyce *et al.* (2024) show that all cratonic lithosphere is comprised of a positively radially anisotropic upper layer, best explained by Archean underplating and an isotropic layer beneath, indicative of two-stage cratonic keel formation. Our low-azimuthal anisotropy results thus support the notion that Archean terranes are dominated by vertical rather than horizontal modern-day plate tectonics, such as the presence of plumes or crustal delamination and underplating (e.g. Zegers & van Keken 2001; Griffin *et al.* 2003), which would give rise to stratified horizontally oriented fabrics with a large radial, as opposed to azimuthal anisotropy. The high buoyancy and viscosity of cratonic roots, due to their iron-depleted composition, may have allowed for this fabric to persist since Archean times (e.g. Griffin *et al.* 2003; Priestley *et al.* 2020). Multiple layers with a different

anisotropic character can also result in the apparently weak SKS splitting signal (e.g. Debayle *et al.* 2005; Yuan & Romanowicz 2010) observed in Fig. 4, however, as previously discussed, our backazimuthal coverage is not extensive enough to resolve this.

Relatively low δt splits are also present in the Bangweulu Craton (Fig. 4b), with the exception of station LWNG, where only a single PKS measurement of $\delta t \sim 1.5$ s is observed. However, the Bangweulu Craton is Paleoproterozoic in age, and thus younger than the Congo Craton, by which time modern-day plate tectonic processes were already in operation (e.g. Bastow *et al.* 2011; Palin *et al.* 2020).

6 CONCLUSIONS

Using data from the recently deployed CuBES seismograph network and surrounding deployments, we investigate azimuthal anisotropy across the Central African Plateau using shear-wave splitting analysis of SKS, SKKS and PKS phases. Results reveal complex lithospheric deformation fabrics across the region's Pan-African orogenic belts and shear zones. A schematic summary of the main observations and interpretations is shown in Fig. 7.

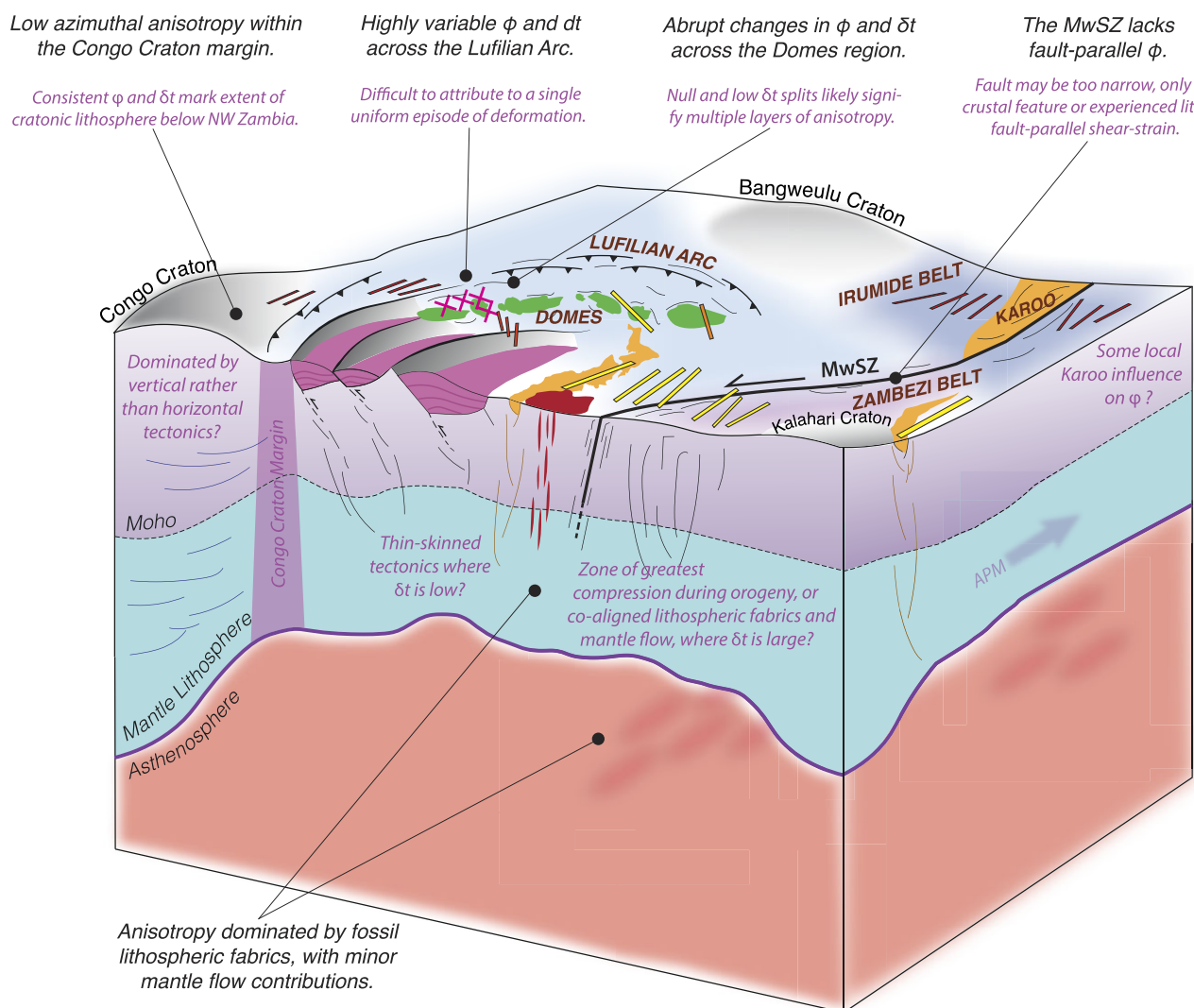


Figure 7. Illustrative diagram summarizing the main observations and interpretations derived from the shear-wave splitting analysis. MwSZ: Mwembeshi shear zone. APM: Absolute plate motion direction. See Fig. 1 for further details on the tectonic provinces.

Highly variable anisotropic fast directions (ϕ) and delay times (δt) over short length-scales (<100 km) suggest fossil lithospheric fabrics, as opposed to sublithospheric mantle flow, dominate the observed anisotropy. The Mwembeshi shear zone, which separates two regions of distinct lithological characteristics at the surface, is not associated with fault-parallel ϕ , indicating the fault is either too narrow to be discernible in our SKS splitting analysis, or too thin-skinned to have left an imprint at mantle lithospheric depths. Alternatively, it may have experienced little fault-parallel shear strain during its latest active phase as a sinistral strike-slip fault, and thus unable to form sufficient mantle olivine alignment. In the heart of the Lufilian Arc, we observe abrupt changes in splitting parameters (NE–SW, N–S and NW–SE): no single uniform, anisotropic fabric defines the entire region. This is consistent with the view that multiple episodes of deformation shaped the Lufilian Arc, or perhaps that pre-existing fabrics, relating to Neoproterozoic Katangan Basin development, have failed to be completely overprinted by the Pan-African orogeny. Near the Domes, where most intense crustal re-working is thought to have taken place during the orogeny, relatively large anisotropic splitting measurements ($\delta t > 1$ s) surround a cluster of predominantly null and low δt (<0.7 s) splits that reflect the lack of organized LPO fabrics and thus likely the presence of depth-dependent anisotropy. During their early-Paleozoic development in the Pan-African orogeny, these complex anisotropic zones may have manifest as fault and fracture networks, ultimately facilitating the fluid migration required for the region's copper-rich mineralization. Consistently weak anisotropy (low $\delta t < 0.7$ s) within the Congo Craton margin supports the notion that some Archean terranes are dominated by vertical rather than horizontal tectonics.

ACKNOWLEDGMENTS

We thank the editor and two anonymous reviewers who prompted us to think more deeply about lower mantle anisotropy and the development of the Mwembeshi shear zone. We thank the SEIS-UK data management facility for providing seismograph instruments for the CuBES deployment in Zambia and thank L. Finch, V. Lane, T. Mackay-Champion, M. Mutale, G. Shiyanga, A. Ngulube and M. Chifita for their valuable fieldwork assistance during the installation and maintenance of the network. We acknowledge collaboration with the Zambian Ministry of Mines and their help in establishing the CuBES seismograph network, as well as First Quantum Minerals (FQM) and Kalahari GeoEnergy for their logistical help during fieldwork. We also acknowledge support from the wider Basin Analysis and Multi-Physics on the Central African Copper Belt (CACB) group led by the Department of Earth Sciences at the University of Oxford. This work was supported by the Natural Environment Research Council grant number NE/T003170/1 (CuBES WP1). Seismic Analysis Code (SAC; Helffrich *et al.* 2013) and Generic Mapping Tools (GMT; Wessel & Smith 1998) software were used to process and display seismic data. We thank James Wookey for making the shear-wave splitting source code freely available online at <https://github.com/jwooley/sheba>. For the purpose of open access, the author has applied a Creative Commons Attribution (CC BY) licence to any Author Accepted Manuscript (AAM) version arising.

SUPPORTING INFORMATION

Supplementary data are available at [GJI](https://doi.org/10.1093/gji/gjaa346) online.

Table S1: Broad-band seismograph stations deployed in the CuBES project for an 18-month period, until late 2023 November/early

December. The symbols in the first column correspond to those used in Figure 1B to denote the CuBES network.

Table S2: Shear-wave splitting measurements for the CuBES network. δt (s) is the time delay between the fast and slow shear waves. ϕ is the orientation of the fast shear wave (measured in degrees clockwise from north). σ is the error associated with each parameter.

Table S3: Shear-wave splitting measurements for additional stations across the Central African Plateau. δt (s) is the time delay between the fast and slow shear waves. ϕ is the orientation of the fast shear wave (measured in degrees clockwise from north). σ is the error associated with each parameter.

Please note: Oxford University Press is not responsible for the content or functionality of any supporting materials supplied by the authors. Any queries (other than missing material) should be directed to the corresponding author for the paper.

CONFLICT OF INTEREST

The authors declare that they have no known competing financial interests or personal relationships that could have appeared to influence the work reported in this paper.

DATA AVAILABILITY

The facilities of EarthScope Consortium were used for access to waveforms, related metadata, and/or derived products used in this study. These services are funded through the National Science Foundation's Seismological Facility for the Advancement of Geoscience (SAGE) Award under Cooperative Agreement EAR-1724509. All seismic data were downloaded through the EarthScope Consortium Web Services (<https://service.iris.edu/>) for the following networks: the ZP (Nyblade 2007), AF (Penn State University 2004), BX (Botswana Geoscience Institute 2001), XK (Gao *et al.* 2012) and IU (Albuquerque Seismological Laboratory/U. S. Geological Survey 2014) networks.

REFERENCES

- Afonso, J.C. *et al.*, 2022. Thermochemical structure and evolution of cratonic lithosphere in central and southern Africa, *Nat. Geosci.*, **15**(5), 405–410.
- Albuquerque Seismological Laboratory/U. S. Geological Survey, 2014. Global Seismograph Network (GSN - IRIS/USGS) [Data set], International Federation of Digital Seismograph Networks, <https://doi.org/10.7914/SN/AF> (accessed 13th March 2024).
- Alsina, D. & Snieder, R., 1995. Small-scale sublithospheric continental mantle deformation: constraints from SKS splitting observations, *Geophys. J. Int.*, **123**(2), 431–448.
- Andriampenomanana, F. *et al.*, 2024. Coherent seismic anisotropy pattern across southern Africa revealed by shear wave splitting measurements, *Earth Space Sci.*, **11**(5), e2023EA003469, doi:10.1029/2023EA003469.
- Bagley, B. & Nyblade, A.A., 2013. Seismic anisotropy in eastern Africa, mantle flow, and the African superplume, *Geophys. Res. Lett.*, **40**(8), 1500–1505.
- Banks, N., Bardwell, K. & Musiwa, S., 1995. Karoo rift basins of the Luangwa Valley, Zambia, *Geol. Soc. Lond. Spec. Publ.*, **80**(1), 285–295.
- Barruol, G. & Ismail, W.B., 2001. Upper mantle anisotropy beneath the African IRIS and Geoscope stations, *Geophys. J. Int.*, **146**(2), 549–561.
- Barruol, G. & Mainprice, D., 1993. A quantitative evaluation of the contribution of crustal rocks to the shear-wave splitting of teleseismic SKS waves, *Phys. Earth Planet. Int.*, **78**(3–4), 281–300.

- Bastow, I.**, Owens, T., Helffrich, G. & Knapp, J., 2007. Spatial and temporal constraints on sources of seismic anisotropy: evidence from the Scottish highlands, *Geophys. Res. Lett.*, **34**(5), doi:10.1029/2006GL028911.
- Bastow, I.D.**, Thompson, D.A., Wookey, J., Kendall, J.-M., Helffrich, G., Snyder, D.B., Eaton, D.W. & Darbyshire, F.A., 2011. Precambrian plate tectonics: seismic evidence from northern Hudson Bay, Canada, *Geology*, **39**(1), 91–94.
- Batumike, J.**, Griffin, W., Belousova, E., Pearson, N., O'Reilly, S.Y. & Shee, S., 2008. LAM-ICPMS U–Pb dating of kimberlitic perovskite: eocene–oligocene kimberlites from the Kundelungu Plateau, DR Congo, *Earth Planet. Sci. Lett.*, **267**(3–4), 609–619.
- Botswana Geoscience Institute**, 2001. Botswana Seismological Network [Data set], International Federation of Digital Seismograph Networks. <https://doi.org/10.7914/SN/BX> (accessed 13th March 2024).
- Boyce, A.**, Bastow, I.D., Cottar, S., Kounoudis, R., Guilloud De Courbeville, J., Caunt, E. & Desai, S., 2021. AFRP20: new P-wavespeed model for the African mantle reveals two whole-mantle plumes below East Africa and neoproterozoic modification of the tanzania craton, *Geochem. Geophys. Geosyst.*, **22**, e2020GC009302, doi:10.1029/2020GC009302.
- Boyce, A.**, Bodin, T., Durand, S., Soergel, D. & Debayle, E., 2024. Seismic evidence for craton formation by underplating and development of the MLD, *Geophys. Res. Lett.*, **51**(4), e2023GL106170, doi:10.1029/2023GL106170.
- Catuneanu, O.**, Wopfner, H., Eriksson, P., Cairncross, B., Rubidge, B., Smith, R. & Hancox, P., 2005. The karoo basins of south-central Africa, *J. Afr. Earth Sci.*, **43**(1–3), 211–253.
- Chen, Y.** & Niu, F., 2016. Joint inversion of receiver functions and surface waves with enhanced preconditioning on densely distributed CNDSN stations: crustal and upper mantle structure beneath China, *J. Geophys. Res. Solid Earth*, **121**(2), 743–766.
- Cosi, M.**, De Bonis, A., Goso, G., Hunziker, J., Martinotti, G., Moratto, S., Robert, J. & Ruhlman, F., 1992. Late Proterozoic thrust tectonics, high-pressure metamorphism and uranium mineralization in the Domes area, Lufilian Arc, northwestern Zambia, *Precambrian Res.*, **58**(1–4), 215–240.
- Coward, M.** & Daly, M.C., 1984. Crustal lineaments and shear zones in Africa: their relationship to plate movements, *Precambrian Res.*, **24**(1), 27–45.
- Craig, T.**, Jackson, J., Priestley, K. & McKenzie, D., 2011. Earthquake distribution patterns in Africa: Their relationship to variations in lithospheric and geological structure, and their rheological implications, *Geophys. J. Int.*, **185**(1), 403–434.
- Daly, M.C.**, 1986. The intracratonic Irumide belt of Zambia and its bearing on collision orogeny during the Proterozoic of Africa, *Geol. Soc. Lond. Spec. Publ.*, **19**(1), 321–328.
- Daly, M.C.**, Green, P., Watts, A., Davies, O., Chibesakunda, F. & Walker, R., 2020. Tectonics and landscape of the Central African Plateau and their implications for a propagating Southwestern Rift in Africa, *Geochem. Geophys. Geosyst.*, **21**(6), e2019GC008746, doi:10.1029/2019GC008746.
- Daly, M.C.**, 1988. Crustal shear zones in Central Africa: a kinematic approach to Proterozoic tectonics, *Episodes J. Int. Geosci.*, **11**(1), 5–11.
- De Plaen, R.**, Bastow, I., Chambers, E., Keir, D., Gallacher, R. & Keane, J., 2014. The development of magmatism along the Cameroon Volcanic Line: evidence from seismicity and seismic anisotropy, *J. Geophys. Res. Solid Earth*, **119**(5), 4233–4252.
- de Swardt, A.J.**, Garrard, P. & Simpson, J., 1965. Major zones of transcurrent dislocation and superposition of orogenic belts in part of central Africa, *Geol. Soc. Am. Bull.*, **76**(1), 89–102.
- Debayle, E.** & Ricard, Y., 2013. Seismic observations of large-scale deformation at the bottom of fast-moving plates, *Earth Planet. Sci. Lett.*, **376**, 165–177.
- Debayle, E.**, Kennett, B. & Priestley, K., 2005. Global azimuthal seismic anisotropy and the unique plate-motion deformation of Australia, *Nature*, **433**(7025), 509–512.
- Delvaux, D.** & Barth, A., 2010. African stress pattern from formal inversion of focal mechanism data, **482**(1–4), 105–128.
- Díaz, J.** & Gallart, J., 2014. Seismic anisotropy from the Variscan core of Iberia to the Western African Craton: new constraints on upper mantle flow at regional scales, *Earth Planet. Sci. Lett.*, **394**, 48–57.
- Ebinger, C.**, Reiss, M.C., Bastow, I. & Karanja, M.M., 2024. Shallow sources of upper mantle seismic anisotropy in East Africa, *Earth Planet. Sci. Lett.*, **625**, 118 488.
- Ebinger, C.J.** & Sleep, N.H., 1998. Cenozoic magmatism throughout east Africa resulting from impact of a single plume, *Nature*, **395**(6704), 788, doi:10.1038/27417.
- Eglinger, A.**, Vanderhaeghe, O., André-Mayer, A.-S., Goncalves, P., Zeh, A., Durand, C. & Deloule, E., 2016. Tectono-metamorphic evolution of the internal zone of the Pan-African Lufilian orogenic belt (Zambia): implications for crustal reworking and syn-orogenic uranium mineralizations, *Lithos*, **240**, 167–188.
- Elsheikh, A.A.**, 2019. Seismic anisotropy and mantle flow beneath East Africa and Arabia, *J. Afr. Earth Sci.*, **149**, 97–108.
- Emry, E.L.**, Shen, Y., Nyblade, A.A., Flinders, A. & Bao, X., 2019. Upper mantle Earth structure in Africa from full-wave ambient noise tomography, *Geochem. Geophys. Geosyst.*, **20**(1), 120–147.
- Forte, A.M.**, Quéré, S., Moucha, R., Simmons, N.A., Grand, S.P., Mitrovica, J.X. & Rowley, D.B., 2010. Joint seismic–geodynamic–mineral physical modelling of African geodynamics: a reconciliation of deep-mantle convection with surface geophysical constraints, *Earth Planet. Sci. Lett.*, **295**(3–4), 329–341.
- Fouch, M.J.** & Rondenay, S., 2006. Seismic anisotropy beneath stable continental interiors, *Phys. Earth Planet. Int.*, **158**(2–4), 292–320.
- Fritz, H.** et al., 2013. Orogen styles in the East African Orogen: a review of the Neoproterozoic to Cambrian tectonic evolution, *J. Afr. Earth Sci.*, **86**, 65–106.
- Gao, S.**, Liu, K., Abdelsalam, M. & John, H., 2012. Seismic arrays for african rift initiation [Data set], International Federation of Digital Seismograph Networks. https://doi.org/10.7914/SN/XK_2012 (accessed 14th March 2024).
- Gilligan, A.** et al., 2016. Lithospheric deformation in the Canadian Appalachians: evidence from shear wave splitting, *Geophys. J. Int.*, **206**(2), 1273–1280.
- Glynn, S.M.**, Master, S., Wiedenbeck, M., Davis, D.W., Kramers, J.D., Belyanin, G.A., Frei, D. & Oberthür, T., 2017. The Proterozoic Choma-Kalomo block, SE Zambia: exotic terrane or a reworked segment of the Zimbabwe craton?, *Precambrian Res.*, **298**, 421–438.
- Griffin, W.**, O'Reilly, S., Abe, N., Aulbach, S., Davies, R., Pearson, N., Doyle, B. & Kivi, K., 2003. The origin and evolution of Archean lithospheric mantle, *Precambrian Res.*, **127**(1–3), 19–41.
- Hansen, S.E.**, Nyblade, A.A. & Benoit, M.H., 2012. Mantle structure beneath Africa and Arabia from adaptively parameterized P-wave tomography: Implications for the origin of Cenozoic Afro-Arabian tectonism, *Earth Planet. Sci. Lett.*, **319**, 23–34.
- Hanson, R.E.**, Wilson, T.J. & Wardlaw, M.S., 1988. Deformed batholiths in the Pan-African Zambezi belt, Zambia: age and implications for regional Proterozoic tectonics, *Geology*, **16**(12), 1134–1137.
- Hanson, R.E.**, Wilson, T.J. & Munyanyiwa, H., 1994. Geologic evolution of the Neoproterozoic Zambezi orogenic belt in Zambia, *J. Afr. Earth Sci.*, **18**(2), 135–150.
- Helffrich, G.**, Wookey, J. & Bastow, I.D., 2013. *The Seismic Analysis Code: A Primer and User's Guide*, Cambridge University Press, Cambridge.
- James, D.** & Fouch, M., 2002. Formation and evolution of Archaean cratons: insights from southern Africa, *Geol. Soc. Lond. Spec. Publ.*, **199**(1), 1–26.
- John, T.** & Schenk, V., 2003. Partial eclogitisation of gabbroic rocks in a late Precambrian subduction zone (Zambia): prograde metamorphism triggered by fluid infiltration, *Contrib. Mineral. Petrol.*, **146**, 174–191.
- John, T.**, Schenk, V., Mezger, K. & Tembo, F., 2004. Timing and PT evolution of whiteschist metamorphism in the Lufilian Arc–Zambezi Belt orogen (Zambia): implications for the assembly of Gondwana, *J. Geol.*, **112**(1), 71–90.
- Kachingwe, M.**, Nyblade, A. & Julia, J., 2015. Crustal structure of Precambrian terranes in the southern African subcontinent with implications for secular variation in crustal genesis, *Geophys. J. Int.*, **202**(1), 533–547.
- Kampunzu, A.** & Cailteux, J., 1999. Tectonic evolution of the Lufilian arc (Central Africa Copper Belt) during Neoproterozoic Pan African orogenesis, *Gondwana Res.*, **2**(3), 401–421.

- Kendall, J.-M.**, Stuart, G.W., Ebinger, C.J., Bastow, I.D. & Keir, D., 2005. Magma-assisted rifting in Ethiopia, *Nature*, **433**(7022), 146–148.
- Kendall, J.-M.**, Pilidou, S., Keir, D., Bastow, I.D., Stuart, G.W. & Ayele, A., 2006. Mantle upwellings, melt migration and the rifting of Africa: Insights from seismic anisotropy, *Geol. Soc. Lond. Spec. Publ.*, **259**, 271–293.
- Kennett, B.L.N.**, Engdahl, E.R. & Buland, R., 1995. Constraints on seismic velocities in the Earth from travel-times, *Geophys. J. Int.*, **122**(1), 108–124.
- Key, R.**, Liyungu, A., Njamu, F.M., Somwe, V., Banda, J., Mosley, P. & Armstrong, R., 2001. The western arm of the Lufilian Arc in NW Zambia and its potential for copper mineralization, *J. Afr. Earth Sci.*, **33**(3–4), 503–528.
- Kipata, M.L.**, Delvaux, D., Sebaggenzi, M.N., Cailteux, J. & Sintubin, M., 2013. Brittle tectonic and stress field evolution in the Pan-African Lufilian arc and its foreland (Katanga, DRC): from orogenic compression to extensional collapse, transpressional inversion and transition to rifting., *Geol. Belg.*, **16**(1–2), 001–017.
- Ko, B.** & Jung, H., 2015. Crystal preferred orientation of an amphibole experimentally deformed by simple shear, *Nat. Commun.*, **6**(1), 6586, doi:10.1038/ncomms7586.
- Kreemer, C.**, Blewitt, G. & Klein, E.C., 2014. A geodetic plate motion and global strain rate model, *Geochem. Geophys. Geosyst.*, **15**(10), 3849–3889.
- Lekić, V.** & Romanowicz, B., 2011. Inferring upper-mantle structure by full waveform tomography with the spectral element method, *Geophys. J. Int.*, **185**(2), 799–831.
- Liddell, M.V.**, Bastow, I., Darbyshire, F., Gilligan, A. & Pugh, S., 2017. The formation of Laurentia: evidence from shear wave splitting, *Earth Planet. Sci. Lett.*, **479**, 170–178.
- Liu, J.** & Cao, S., 2023. Development of amphibole crystal preferred orientations (CPOs) and their effects on seismic anisotropy in deformed amphibolites, *J. Geophys. Res. Solid Earth*, **128**(4), e2022JB026136, doi:10.1029/2022JB026136.
- Merry, T.**, Bastow, I., Kounoudis, R., Ogden, C., Bell, R. & Jones, L., 2021. The influence of the north anatolian fault and a fragmenting slab architecture on upper mantle seismic anisotropy in the eastern mediterranean, *Geochem. Geophys. Geosyst.*, **22**(9), e2021GC009896, doi:10.1029/2021GC009896.
- Merry, T.A.** & Eakin, C.M., 2024. Insights on the African upper mantle from Quasi-Love wave scattering, *Geochem. Geophys. Geosyst.*, **25**(4), e2023GC011385, doi:10.1029/2023GC011385.
- Naydenov, K.V.**, Lehmann, J., Saalmann, K., Milani, L., Kinnaird, J.A., Charlesworth, G., Frei, D. & Rankin, W., 2014. New constraints on the pan-African orogeny in central zambia: a structural and geochronological study of the hook batholith and the mwembeshi zone, *Tectonophysics*, **637**, 80–105.
- Nyblade, A.**, 2007. Africa Array- Uganda/Tanzania [Data Set], International Federation of Digital Seismograph Networks. https://doi.org/10.7914/SN/ZP_2007 (accessed 13th March 2024).
- Ogden, C.**, Holwell, D., Daly, M., Chifwepa, C., T, M.-C. & S, F., 2022. The copper basin exploration science project: examining the crustal structure of Zambia using broadband seismology, *British Seismology Meeting (BSM)*.
- Palin, R.M.**, Santosh, M., Cao, W., Li, S.-S., Hernández-Uribe, D. & Parsons, A., 2020. Secular change and the onset of plate tectonics on Earth, *Earth-Sci. Rev.*, **207**, 103 172, doi:10.1016/j.earscirev.2020.103172.
- Penn State University**, 2004. AfricaArray [Data set], International Federation of Digital Seismograph Networks.<https://doi.org/10.7914/SN/AF> (accessed 13th March 2024).
- Porada, H.**, 1989. Pan-African rifting and orogenesis in southern to equatorial Africa and eastern Brazil, *Precambrian Res.*, **44**(2), 103–136.
- Porada, H.** & Berhorst, V., 2000. Towards a new understanding of the neoproterozoic-early palaeozoic lufilian and northern zambezi belts in zambia and the democratic Republic of Congo, *J. Afr. Earth Sci.*, **30**(3), 727–771.
- Priestley, K.**, McKenzie, D. & Ho, T., 2018. A lithosphere–asthenosphere boundary—a global model derived from multimode surface-wave tomography and petrology, *Lithospheric Discontinuities*, pp. 111–123, American Geophysical Union, Washington, D.C., USA.
- Priestley, K.**, Ho, T. & McKenzie, D., 2020. The formation of continental roots, *Geology*, **49**(2), 190–194.
- Rainaud, C.**, Master, S., Armstrong, R. & Robb, L., 2003. A cryptic Mesoarchean terrane in the basement to the Central African Copperbelt, *J. Geol. Soc.*, **160**(1), 11–14.
- Reed, C.A.**, Liu, K.H., Yu, Y. & Gao, S.S., 2017. Seismic anisotropy and mantle dynamics beneath the Malawi Rift Zone, East Africa, *Tectonics*, **36**(7), 1338–1351.
- Reiss, M.**, Rümpker, G., Tilman, F., Yuan, X., Giese, J. & Rindraharisaona, E.J., 2016. Seismic anisotropy of the lithosphere and asthenosphere beneath southern Madagascar from teleseismic shear wave splitting analysis and waveform modeling, *J. Geophys. Res. Solid Earth*, **121**(9), 6627–6643.
- Reiss, M.**, Long, M. & Creasy, N., 2019. Lowermost mantle anisotropy beneath Africa from differential SKS-SKKS shear-wave splitting, *J. Geophys. Res. Solid Earth*, **124**(8), 8540–8564.
- Restivo, A.** & Helffrich, G., 1999. Teleseismic shear wave splitting measurements in noisyenvironments, *Geophys. J. Int.*, **137**(3), 821–830.
- Restivo, A.** & Helffrich, G., 2006. Core–mantle boundary structure investigated using SKS and SKKS polarization anomalies, *Geophys. J. Int.*, **165**(1), 288–302.
- Sarafian, E.**, Evans, R.L., Abdelsalam, M.G., Atekwana, E., Elsenbeck, J., Jones, A.G. & Chikambwe, E., 2018. Imaging Precambrian lithospheric structure in Zambia using electromagnetic methods, *Gondwana Res.*, **54**, 38–49.
- Savage, M.K.**, 1999. Seismic anisotropy and mantle deformation: what have we learned from shear wave splitting?, *Rev. Geophys.*, **37**(1), 65–106.
- Silver, P.G.**, 1996. Seismic anisotropy beneath the continents: probing the depths of geology, *Annu. Rev. Earth Planet. Sci.*, **24**(1), 385–432.
- Silver, P.G.** & Chan, W.W., 1991. Shear wave splitting and subcontinental mantle deformation, *J. Geophys. Res. Solid Earth*, **96**(B10), 16 429–16 454.
- Silver, P.G.** & Savage, M.K., 1994. The interpretation of shear-wave splitting parameters in the presence of two anisotropic layers, *Geophys. J. Int.*, **119**(3), 949–963.
- Sleep, N.H.**, Ebinger, C.J. & Kendall, J.-M., 2002. Deflection of mantle plume material by cratonic keels, *Geol. Soc. Lond. Spec. Publ.*, **199**(1), 135–150.
- Teanby, N.A.**, Kendall, J.-M. & Van der Baan, M., 2004. Automation of shear-wave splitting measurements using cluster analysis, *Bull. seism. Soc. Am.*, **94**(2), 453–463.
- Thieme, J.G.** & Johnson, R.L., 1981. The Geological Map of the Republic of Zambia, 1:1,000,000. Geological Survey Department, Ministry of Mines, Lusaka, Zambia.
- Tommasi, A.**, Mainprice, D., Canova, G. & Chastel, Y., 2000. Viscoplastic self-consistent and equilibrium-based modeling of olivine lattice preferred orientations: Implications for the upper mantle seismic anisotropy, *J. Geophys. Res. Solid Earth*, **105**(B4), 7893–7908.
- Unrug, R.**, 1983. The Lufilian Arc: a microplate in the Pan-African collision zone of the Congo and the Kalahari cratons, *Precambrian Res.*, **21**(3–4), 181–196.
- Vauchez, A.**, Tommasi, A. & Mainprice, D., 2012. Faults (shear zones) in the Earth's mantle, *Tectonophysics*, **558**, 1–27.
- Walsh, E.**, Arnold, R. & Savage, M., 2013. Silver and Chan revisited, *J. Geophys. Res. Solid Earth*, **118**(10), 5500–5515.
- Ward, J.**, Nowacki, A. & Rost, S., 2020. Lateral velocity gradients in the African lower mantle inferred from slowness space observations of multipathing, *Geochem. Geophys. Geosyst.*, **21**(8), e2020GC009025, doi:10.1029/2020GC009025.
- Wedmore, L.N.**, Turner, T., Biggs, J., Williams, J.N., Sichingabula, H.M., Kabumbu, C. & Banda, K., 2022. The Luangwa Rift Active Fault Database and fault reactivation along the southwestern branch of the East African Rift, *Solid Earth*, **13**(11), 1731–1753.

- Wessel, P.** & Smith, W.H.F., 1998. New, improved version of Generic Mapping Tools released, *EOS Trans. AGU*, **79**(47), 579–579.
- Xu, K.**, Xie, W., Sun, K., Ren, J., Gong, P., He, S., Lu, Y. & Zhang, H., 2022. Geochronology, geochemistry, and petrogenesis of I-and A-type granites in the Solwezi Dome of the Lufilian Arc: implications for the late-Mesoproterozoic magmatic and geodynamic evolution in northern Zambia, *Arab. J. Geosci.*, **15**(23), 1729, doi:10.1007/s12517-022-10971-0.
- Yuan, H.** & Romanowicz, B., 2010. Lithospheric layering in the North American craton, *Nature*, **466**(7310), 1063–1068.
- Zegers, T.E.** & van Keeken, P.E., 2001. Middle Archean continent formation by crustal delamination, *Geology*, **29**(12), 1083–1086.
- Zhang, S.** & Karato, S.-I., 1995. Lattice preferred orientation of olivine aggregates deformed in simple shear, *Nature*, **375**(6534), 774–777.